Minimal Kinetic Mechanism for Misincorporation by DNA Polymerase I (Klenow Fragment)†

Bryan T. Eger and Stephen J. Benkovic*

152 Davey Laboratory, Department of Chemistry, The Pennsylvania State University, University Park, Pennsylvania 16802

Received March 27, 1992; Revised Manuscript Received June 24, 1992

ABSTRACT: The minimal kinetic mechanism for misincorporation of a single nucleotide (dATP) into a short DNA primer/template (9/20-mer) by the Klenow fragment of DNA polymerase I [KF(exo+)] has been previously published [Kuchta, R. D., Benkovic, P., & Benkovic, S. J. (1988) *Biochemistry 27*, 6716–6725]. In this paper are presented refinements to this mechanism. Pre-steady-state measurements of correct nucleotide incorporation (dTTP) in the presence of a single incorrect nucleotide (dATP) with excess KF(exo+) demonstrated that dATP binds to the KF(exo+)–9/20-mer complex in two steps preceding chemistry. Substitution of (αS)dATP for dATP yielded identical two-step binding kinetics, removing nucleotide binding as a cause of the elemental effect on the rate of misincorporation. Pyrophosphate release from the ternary species [KF′(exo+)–9A/20-mer-PP_i] was found to occur following a rate-limiting conformational change, with this species partitioning equally to either nucleotide via internal pyrophosphorolysis or to misincorporated product. The rate of 9A/20-mer dissociation from the central ternary complex (KF′–9A/20-mer–PP_i) was shown to be negligible relative to exonucleolytic editing. Pyrophosphorolysis of the misincorporated DNA product (9A/20-mer), in conjunction with measurement of the rate of dATP misincorporation, permitted determination of the overall equilibrium constant for dATP misincorporation and provided a value similar to that measured for correct incorporation. A step by step comparison of the polymerization catalyzed by the Klenow fragment for correct and incorrect nucleotide incorporation emphasizes that the major source of the enzyme's replicative fidelity arises from discrimination in the actual chemical step and from increased exonuclease activity on the ternary misincorporated product complex owing to its slower passage through the turnover sequence.

DNA polymerase I (Pol I)[1] from *Escherichia coli* is a multifunctional, monomeric, DNA-dependent DNA polymerase involved in replication and repair synthesis (Kornberg & Baker, 1992). Pol I replicates DNA with high fidelity, making one mispairing for every 10^6–10^8 bases incorporated (Englisch et al., 1985). The enzyme contains three separate domains which catalyze polymerase, 3′→5′ exonuclease, and 5′→3′ exonuclease activities. Removal of the 5′→3′ exonuclease domain either by protease degradation (Brutlag et al., 1969; Klenow & Henningsen, 1970) or by mutation (Joyce & Grindley, 1983) generates an enzyme known as the Klenow fragment [KF(exo+)], which contains complete polymerase and 3′→5′ exonuclease activities. Recently, a double mutant of the Klenow fragment (Asp355Ala; Glu357Ala) [KF(exo–)] was constructed and shown to have greatly reduced 3′→5′ exonuclease activity while retaining full polymerase activity (Derbyshire et al., 1988).

The Klenow fragment is ideal for study due to its small size, slow polymerization rate, and lack of accessory proteins (Carroll & Benkovic, 1990). In addition to structural (Ollis et al., 1985; Joyce & Steitz, 1987; Freemont et al., 1988; Cowart et al., 1989; Catalano & Benkovic, 1989) and stereochemical studies (Burgers & Eckstein, 1979; Brody & Frey, 1981; Gupta & Benkovic, 1984), extensive kinetic studies have been reported using both Pol I and the Klenow fragment (McClure & Jovin, 1975; Bambara et al., 1976; Bryant et al., 1983; Mizrahi et al., 1985, 1986a,b; Kuchta et al., 1987; Eger et al., 1991; Dahlberg & Benkovic, 1991). In recent publications from our laboratory, the minimal kinetic mechanism for the incorporation of either a single correct nucleotide (Kuchta et al., 1987) or a single incorrect nucleotide (Kuchta et al., 1988) had been determined. From a comparison of these two mechanisms the fidelity of DNA replication was shown to be enhanced at three stages during nucleotide incorporation: (i) nucleotide binding and chemistry; (ii) a conformational change preceding pyrophosphate release (internal proofreading); and (iii) addition of the next nucleotide onto a mismatch (external proofreading) (Kuchta et al., 1988). We now present five additional experiments which allow for further refinement of the kinetic mechanism for misincorporation: (i) nucleotide discrimination experiments to measure the binding sequence of an incorrect dATP to the KF–DNA species; (ii) pyrophosphorolysis experiments to measure the overall equilibrium of the misincorporation reaction; (iii) pyrophosphate release experiments to measure the rate at which pyrophosphate is lost following a chemical step involving misincorporation; (iv) nucleotide discrimination to determine the effect of elemental substitution [(S_p)-α-thio-dATP] on the binding of dATP to the KF–DNA complex; and (v) steady-state nucleotide turnover to examine internal proofreading on the ternary product complex.

EXPERIMENTAL PROCEDURES

Materials. Sodium pyrophosphate and yeast inorganic pyrophosphatase were purchased from Sigma. The purity of the pyrophosphate was determined to be >98% by ^{31}P NMR.

† This work was supported by NIH Grant GM13306 (S.J.B.).

* Address correspondence to this author.

[1] Abbreviations: Pol I, DNA polymerase I; KF(exo+), Klenow fragment of DNA polymerase I; KF(exo–), a double mutant (Asp355Ala, Glu357Ala) of the Klenow fragment with reduced 3′→5′ exonuclease activity; TEAB, triethylammonium bicarbonate; PP_i, sodium pyrophosphate; KP_i, potassium phosphate; Tris-HCl, Tris(hydroxymethyl)aminomethane, hydrochloride salt; HCl, hydrochloric acid; EDTA, ethylenediaminetetraacetate; cpm, counts per minute.

0006-2960/92/0431-9227$03.00/0

Radioactive compounds were purchased from New England Nuclear. DNA was purchased from American Synthesis Inc.

Purity of Radioactive Stocks. The purity of the (α^{32}P)-dNTP was determined by TLC immediately before use. The (α^{32}P)dNTP ($\sim 1 \times 10^5$ cpm) along with authentic nucleoside mono-, di-, and triphosphates ($\sim$10 nmol each) was spotted in triplicate on PEI–cellulose F TLC plates (EM Science) and eluted with 0.3 M KP_i, pH 7.0. Following autoradiography with XAR-5 film (Kodak) the (α^{32}P)dNTP purity was determined by cutting the plate into appropriate sections and counting them in ScintiVerse II (Fisher) in either an LS6800 or LS8100 scintillation counter (Beckman). The purity of the (^{32}P)PP_i was determined similarly. The identities of the PP_i and P_i species were determined by incubation of the (^{32}P)PP_i with pyrophosphatase under conditions appropriate for hydrolysis of all (^{32}P)PP_i and quantitation by TLC as described above.

Additional Nucleotides. Nonradioactive nucleotides were purchased from Sigma or Pharmacia. The (αS)dATP was synthesized according to published procedures (Chen & Benkovic, 1983), and the purity was determined to be >99% by HPLC immediately before use.

Klenow Fragment. The KF(exo+) was purified according to published procedures (Joyce & Grindley, 1983). The KF(exo–), which was also purified by published procedures (Derbyshire et al., 1988), was further purified by chromatography on a Bio-Rex 70 (Bio-Rad) column which had been equilibrated with 10 mM KP_i, pH 7.0. Protein was eluted with a 300-mL linear gradient of 0–1 M KCl in 10 mM KP_i, pH 7.0. The column fractions containing KF(exo–), as determined by absorbance at 278 nm, were loaded onto a Sephadex G-150 column (Pharmacia) and eluted with 10 mM KP_i, pH 7.0. The enzyme was concentrated by dialysis against 10 mM KP_i, pH 7.0, 1 mM dithiothreitol, and 50% glycerol. Both the KF(exo–) and KF(exo+) were determined to be >98% pure by sodium dodecyl sulfate–polyacrylamide gel analysis. Enzyme concentrations were determined using $\epsilon_{278} = 6.32 \times 10^4$ M^{-1} cm^{-1} (Setlow et al., 1972). All other materials were of the highest quality commercially available.

DNA. The DNA was purified by sizing on polyacrylamide gel followed by removal from the gel with six elutions (30 min each) of 0.1 M TEAB, pH 7.6. The DNA was loaded onto a DE52 column (Whatman) which had been equilibrated with 0.1 M TEAB, pH 7.6. The column volume used was 1 mL/100 nmol of crude DNA. After the column was washed with equilibration buffer, the DNA was eluted with 1.0 M TEAB, pH 7.6. The DNA was dried and then resuspended in 50 mM Tris-HCl, pH 7.4. The DNA concentrations were determined from the absorption at 260 nm, using a DNA extinction coefficient equal to the sum of the extinction coefficients of each base. DNA duplexes (Chart I) were annealed in a reaction mix containing equal concentrations of primer and template (10 μM each) with 50 mM NaCl and 5 mM $NaCl_2$ in 50 mM Tris-HCl, pH 7.4. After heating to 70° C, the reactions were allowed to cool to room temperature (2–3 h). Accurate DNA concentrations were determined by single nucleotide incorporation using excess KF(exo+) over DNA, at several enzyme concentrations (Bryant et al., 1983).

Chart I: Duplex DNA Sequences

name[a]	sequence
9/20-mer	TCGCAGCCG AGCGTCGGCAGGTTCCCAAA
9A/20-mer	TCGCAGCCGA AGCGTCGGCAGGTTCCCAAA
9A^s/20-mer	TCGCAGCCGAs AGCGTCGGCAGGTTCCCAAA
9C/20-mer	TCGCAGCCGC AGCGTCGGCAGGTTCCCAAA
10/20-mer	TCGCAGCCGT AGCGTCGGCAGGTTCCCAAA
13/20-mer	TCGCAGCCGTCCA AGCGTCGGCAGGTTCCCAAA
14/20-mer	TCGCAGCCGTCCAA AGCGTCGGCAGGTTCCCAAA

[a] The name of each DNA defines the length of the deoxyoligonucleotide used for the primer/template. The primer designations 9A and 9C represent misincorporation onto the 3′-end of the 9-mer primer to form either an A–A or a C–A mismatch. The 9A^S/20-mer contains a single (αS)dAMP incorporated into the 9/20-mer.

Methods

Enzyme Assays. All assays were run with 10 mM free $MgCl_2$ in 50 mM Tris-HCl, pH 7.4, at room temperature (standard conditions) unless otherwise noted.

Gel Electrophoresis. Aliquots (2.5 μL) of reaction solution were quenched into gel load buffer (7.5 μL) [90% formamide, 1 × TBE (45 mM Tris–borate, 1.0 mM EDTA, pH 8.0) 0.25% bromophenol blue, 0.25% xylene cyanol] and separated on denaturing (8 M urea) 10–12% acrylamide gels. Products were quantitated first by exposing and developing XAR-5 film, followed by excising of product bands and scintillation counting in 3 mL of ScintiVerse II (Mizrahi et al., 1986b).

5′-^{32}P-End Labeling of DNA. DNA oligonucleotide duplexes were 5′-^{32}P-end labeled using T7 polynucleotide kinase (U.S. Biochemical Corp.) with (γ^{32}P)ATP (500–3000 Ci/mmol) as previously documented (Mizrahi et al., 1986b). Following enzyme inactivation at 80 °C for 45 min, the DNA duplex was reannealed by cooling slowly to room temperature (2–3 h).

Data Analysis and Computer Simulations. Computer simulations of product formation as a function of time for the kinetic mechanisms presented were performed using a modified version of the program SIMUL (Barshop et al., 1983; Anderson et al., 1988).

Binding of dATP or (αS)dATP to the KF(exo+)–9/20-mer Complex. The kinetic parameters (K_m and k_{cat}) for the incorporation of dTTP into the 9/20-mer to form the 10/20-mer were measured in reactions containing 400 nM KF(exo+), 200 nM 9/20-mer, and 5–30 μM (α^{32}P)dTTP at 22.0 ± 0.1 °C under standard conditions. Reactions were quenched into a final concentration of 73 mM EDTA (250 μL final volume) over a range of reaction times from 0 to 5 s using a rapid quench instrument (Johnson, 1986). Each quenched assay point was spotted onto either a DE81 or GF/C filter disk (Whatman) and analyzed as previously described (Bryant et al., 1983). The binding of dATP to the KF(exo+)–9/20-mer complex was measured with excess enzyme as described above using a single dTTP concentration (5 μM) and various dATP concentrations (50–250 μM) as previously documented (Eger et al., 1991). The binding of (αS)dATP to the KF(exo+)–9/20-mer complex was measured in a reaction containing 125 μM (αS)dATP and 5 μM dTTP under standard conditions as described above for dATP binding.

Parameters for (αS)dATP. Reactions were run with 330 nM KF(exo–), 100 nM 5′(^{32}P)9/20-mer, and 5, 10, 20, 30, or 40 μM (αS)dATP under standard conditions. After reaction times of 0–80 min, aliquots (2.5 μL) were quenched

into load buffer and quantitated by gel electrophoresis as described above.

Effect of dATP Concentration on Misincorporation. Reactions were run with 330 nM KF(exo+), 100 nM 5′(^{32}P)9/20-mer, and 30, 50, 125, or 250 μM dATP under standard conditions (Mizrahi et al., 1985). After reaction times of 0–10 min, aliquots (2.5 μL) were quenched in load buffer and quantitated by gel electrophoresis as described above.

Quench Effect on either dCTP or dATP Misincorporation. For addition of dCTP or dATP, reactions were run as above with 30 μM nucleotide with KF(exo–) and KF(exo+), respectively. Time points (5 μL) were taken from 0 to 3 h (dCTP) or from 0 to 30 min (dATP) and quenched immediately into either EDTA (45 mM final concentration) or HCl (1.0 N final concentration). The enzyme was denatured in chloroform (100 μL) followed by neutralization of the acid-quenched reaction with NaOH. Additional Tris-HCl, pH 7.4, was added (1.0 M), and the sample was dried. Each sample was resuspended in 50% load buffer (135 μL) and quantitated by gel electrophoresis as described above.

Pyrophosphate Off-Rate from the KF(exo–)-9A/20-PPi Complex

Synthesis of (γ^{32}P)dATP. (γ^{32}P)dATP was synthesized in a reaction (80 μL) containing 0.73 unit/μL of nucleoside diphosphate kinase (Sigma), 0.47 μM (γ^{32}P)ATP (3000 Ci/mmol), 94 μM dADP, and 7 mM $MgCl_2$ in 50 mM Tris-HCl, pH 7.4. The reaction mix was incubated at 37 °C for 30 min and then raised to 70 °C for 60 min to denature the kinase. Small aliquots (2.5 μL) of the reaction mix were spotted every 0.5 cm onto a PEI–cellulose F TLC plate. The plate was eluted with 0.3 M KP_i, pH 7.0, and then dried. After exposure and development of XAR-5 film, the section of the plate that contained the nonseparated dATP and ATP species, as identified by authentic markers, was cut out. The nucleotides were removed from the TLC plate by successive elutions (10 min) with 0.1 M TEAB, pH 7.6, and then, to remove colored impurities, loaded onto a DEAE-Sephadex A-50 column (Sigma) (5 mL) which had been equilibrated with 0.1 M TEAB, pH 7.6. The column was washed with the equilibration buffer, and the nucleotides were eluted with 1.0 M TEAB, pH 7.6. The nucleotides were dried, then redissolved in 50 mM Tris-HCl, pH 7.4, and stored at –20 °C.

Since neither the TLC nor the column conditions separated dATP from ATP, HPLC using a μBondapak C_{18} column (Waters) at 260 nm with a flow rate of 1 mL/min, eluting with a 30-min linear gradient of 100% A to 90% B (A, 0.1 M KP_i, pH 6.0; B, methanol) was run on the purified mixture to confirm quantitative label transfer and the stability of the product, (γ^{32}P)dATP, under purification conditions. The identity of the two species was determined by separate injections of each of the authentic nucleotides. Additional authentic dATP and ATP were added to the radiolabeled nucleotides for UV visualization. Column fractions (2 mL) were collected and counted in ScintiVerse II (18 mL). The purity of the radiolabeled dATP was calculated from the percent of radioactivity in the dATP peak relative to the ATP peak.

Kinetic Measurements. The pre-steady-state formation of enzyme-bound and free pyrophosphate from the reaction of (γ^{32}P)dATP with 9/20-mer to form 9A/20-mer was measured in assays containing 1.7 μM 9/20-mer, 4.0 μM KF(exo–), 10–30 μM (γ^{32}P)dATP, and 45 units/μL inorganic pyrophosphatase. The 9/20-mer concentration was measured by single nucleotide incorporation as previously described (Bryant et al., 1983). Aliquots (5 μL) were removed at times ranging from 0 to 10 min and quenched as previously described. Samples were dried at 25 °C (3 h) and then dissolved in 50 mM Tris-HCl, pH 7.4 (15 μL). The samples (2.5 μL) were individually spotted onto PEI–cellulose F TLC plates, eluted with 0.3 M KP_i, pH 7.0, dried, XAR-5 film exposed, and counted. The R_F values for authentic (^{32}P)P_i and (^{32}P)PP_i markers were determined after their addition to quenched (EDTA or HCl) aliquots of the assay time points. (^{32}P)P_i but not (^{32}P)PP_i and (γ^{32}P)dATP was chromatographically resolved under these conditions.

Several control reactions were performed to ensure that the off-rate assays were adequately quenched and that the products were stable under quench and workup conditions. Three solutions containing (^{32}P)P_i, (^{32}P)PP_i, and (γ^{32}P)dATP (5 μL) were prepared. Each solution was used in turn to prepare three samples. The first sample was mixed (45 s) with chloroform (40 μL) and dried at 25 °C (2.5 h) along with an untreated second sample. The residue from both samples was dissolved separately in 50 mM Tris-HCl, pH 7.4 (15 μL), and dried at 25 °C (3 h). The two samples were dissolved in 50 mM Tris-HCl, pH 7.4 (5 μL), along with an untreated third sample and were quantitated by TLC as described above.

An additional control reaction was conducted to demonstrate that the pyrophosphatase was an adequate coupling enzyme. The steady-state parameters (k_{cat} and K_m) were measured in reactions containing 5 nM pyrophosphatase and 0.5–10 μM (^{32}P)PP_i under standard conditions. Reactions were incubated (0–10 min), quenched into HCl, and quantitated by TLC as described above.

Pyrophosphorolysis on the 9A/20-mer. The parameters (k_{cat} and K_m) for pyrophosphorolysis were measured in assays containing 50 nM 5′-^{32}P-end-labeled 9A/20-mer, 150 nM KF(exo–), and 50 μM–1.0 mM PP_i under standard conditions. At times ranging from 0 to 2 h, aliquots were withdrawn and quenched with gel load buffer and quantitated by acrylamide gel as described above. Control experiments to determine the level of remaining 3′→5′ exonuclease activity were run under the same conditions in the absence of pyrophosphate and quantitated as described above.

Nucleotide Turnover. Reactions were run with 60 nM KF(exo+), 10 μM dGTP, 30 μM (α^{32}P)dATP, and either 1.0 or 1.5 μM 9/20-mer under standard assay conditions. The zero points were made in quadruplicate. After reaction times of 10–120 min, aliquots (3.0 μL) were quenched into EDTA (3.0 μL) (45 mM final concentration). Product dAMP was quantitated using PEI–cellulose F TLC plates as described above.

RESULTS

Binding of dATP to the KF(exo+)–9/20-mer Complex. The method used to measure the binding of dATP to the KF(exo+)–9/20-mer complex (Eger et al., 1991) is outlined in Scheme I. The 9/20-mer was preincubated with excess KF(exo+) to form a kinetically competent KF(exo+)–9/20-mer complex. In addition, to prevent DNA degradation by the 3′→5′ exonuclease activity of the KF(exo+), EDTA was included in the preincubation mix. Initially, the pre-steady-state burst rates were measured for various concentrations of the correct nucleotide (dTTP). These reactions measured the rate of incorporation for the addition of the single correct nucleotide (dTTP) into the 9/20-mer to form the 10/20-mer (data not shown). By varying the concentration of dTTP, the K_m and k_{cat} were calculated for this nucleotide. Since all of the reactions were run with excess KF(exo+) over 9/20-mer,

Scheme I

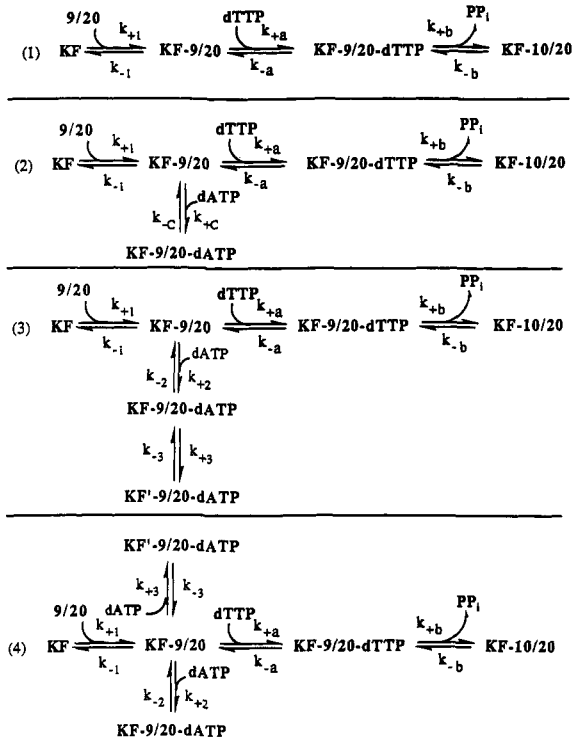

the dTTP incorporation data could be fit to a single exponential, representing the burst of incorporation of dTTP into the 9/20-mer. The data was fit to sequence 1 of Scheme I and yielded values of K_m(dTTP) = 20 μM and k_{cat} = 50 s^{-1}, identical to the data previously published (Eger et al., 1991).

The binding of a single incorrect nucleotide (dATP) to the KF(exo+)–9/20-mer complex was measured by its effect on the rate of correct nucleotide (dTTP) incorporation. Three dATP concentrations ranging from 50 to 250 μM were added to the incorporation reaction while the dTTP concentration was held constant (5 μM). Previous results had demonstrated that dATP will not significantly misincorporate during the 5-s reaction times used in this experiment (Kuchta et al., 1988). Those results ensure that this experiment, known as a nucleotide discrimination experiment, measures only binding of the dATP to the KF(exo+)–9/20-mer complex. The three sets of data were simulated by either a one-step dATP binding (sequence 2 of Scheme I) (Figure 1A) or a two-step dATP binding (sequence 3 of Scheme I) (Figure 1B). The improved fit to sequence 3 provided the values for k_{+2}, k_{-2}, k_{+3}, and k_{-3} listed in Table I and designated in Scheme II.

Binding of (αS)dATP to the KF(exo+)–9/20-mer Complex. In previously published experiments, (αS)dATP had been used to examine both the steady-state elemental effect (6–11) and pre-steady-state elemental effect (65) on misincorporation (Kuchta et al., 1988). Since the nucleotide discrimination experiments allow for direct measurement of the binding of the incorrect nucleotide (dATP), we examined the possibility that part of the elemental effect was due to a decreased binding constant for the α-thio nucleotide relative to the α-oxo nucleotide. The binding of (αS)dATP to the KF–9/20-mer complex, shown in Figure 2, was simulated using both one-step nucleotide binding (sequence 2 of Scheme I) and two-step nucleotide binding (sequence 3 of Scheme I). The good fit to the data for the two-step binding sequence using the identical kinetic constants that describe the behavior of dATP indicates the absence of a sulfur elemental effect in binding.

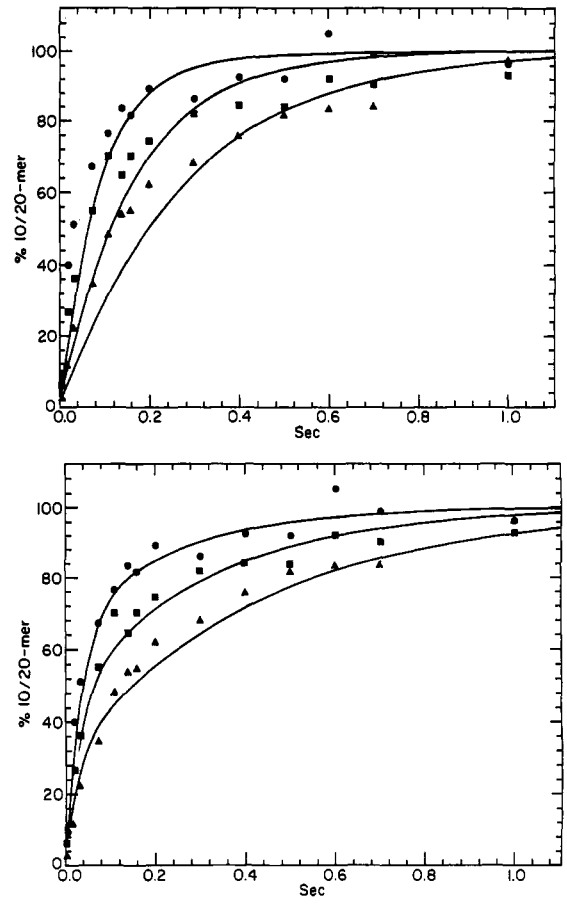

FIGURE 1: Effect of dATP on the pre-steady-state burst of dTTP incorporation into the 9/20-mer to form the 10/20-mer. Assays were performed with excess KF(exo+) as described under Experimental Procedures with 5 μM dTTP and either (●) 50, (■) 125, or (▲) 250 μM dATP. The lines in (A) were generated using sequence 2 of Scheme I and the following individual rate constants: k_{+1} = 1.2 × 10^7 M^{-1} s^{-1}, k_{-1} = 0.06 s^{-1}, k_{+a} = 1 × 10^8 M^{-1} s^{-1}, k_{-a} = 2000 s^{-1}, k_{+b} = 50 s^{-1}, k_{+c} = 1 × 10^8 M^{-1} s^{-1}, and k_{-c} = 2200 s^{-1}. The lines in (B) were generated using sequence 3 of Scheme I with the following rate constants: k_{+2} = 1 × 10^8 M^{-1} s^{-1}, k_{-2} = 1.7 × 10^4 s^{-1}, k_{+3} = 50 s^{-1}, and k_{-3} = 6.5 s^{-1}. The remaining rate constants are equal to those listed above.

Kinetic Parameters for (αS)dATP. The kinetic parameters of (αS)dATP incorporation into the 9/20-mer were measured with excess KF(exo–) over DNA. Values of K_M = 25 ± 4 μM and k_{cat} = 0.0020 ± 0.0004 s^{-1} were obtained from double-reciprocal analysis of single-exponential fits to the burst data (data not shown).

Effect of dATP Concentration on Misincorporation. To examine the catalytic competence of the ternary species formed at high levels of the incorrect nucleotide (dATP), the burst of 9A/20-mer formation was measured under conditions of excess KF(exo+) over 9/20-mer. For concentrations identical to those used for measuring dATP binding (50, 125, and 250 μM), the 9A/20-mer formation showed an increase in both the rate and magnitude of the burst as dATP concentration was increased. These data were simulated to the mechanism in Scheme II and the rate constants in Table I (Figure 3). The burst rate is governed by the rates through step 4, including the first exonuclease step; the burst height reflects the level of KF′–9A/20–PP_i and is sensitive to the values of k_{+5} and k_{exo} (Kuchta et al., 1988).

Quench Effect on either dCTP or dATP Misincorporation. The pre-steady-state misincorporation of dATP into the 9/20-mer to form the 9A/20-mer was measured for KF(exo+) by running parallel reactions which were then quenched

Table I: Fitted Rate Constants for the Misincorporation of dATP into the 9/20-mer To Form the 9A/20-mer

constant	modeled value[a]	ΔG^b (kcal/mol)
$k_{+1}{}^c$ (M^{-1} s^{-1})	1.2×10^7	18.9
$k_{-1}{}^c$ (s^{-1})	6×10^{-2}	18.9
$k_{+2}{}^d$ (M^{-1} s^{-1})	1×10^8	12.7
$k_{-2}{}^d$ (s^{-1})	1.7×10^4	11.6
$k_{+3}{}^d$ (s^{-1})	50	15.0
$k_{-3}{}^d$ (s^{-1})	6.5	16.2
$k_{+4}{}^e$ (s^{-1})	2.5×10^{-2}	19.4
$k_{-4}{}^e$ (s^{-1})	3.0×10^{-3}	20.7
$k_{+5}{}^f$ (s^{-1})	6.0×10^{-3}	20.3
$k_{-5}{}^g$ (s^{-1})	1.4×10^{-4}	22.4
$k_{+6}{}^g$ (s^{-1})	8.0×10^4	10.6
$k_{-6}{}^g$ (M^{-1} s^{-1})	1×10^8	10.6
$k_{+7}{}^c$ (s^{-1})	3.25	16.6
$k_{-7}{}^c$ (M^{-1} s^{-1})	1.2×10^7	16.6
$k_{exo}{}^h$ (s^{-1})	1.1×10^{-2}	

[a] Data were modeled using KINSIM. [b] Free energies were calculated from $\Delta G = RT[\ln (kT/h) - \ln (k_{obs})]$. [c] Data from Kuchta et al. (1988). [d] Data from KINSIM modeling to nucleotide discrimination data. [e] Data from KINSIM modeling to dATP misincorporation and PP_i release data. [f] Data from KINSIM fits to steady-state misincorporation data (Kuchta et al., 1988) and PP_i release data. [g] Data from KINSIM fits to pyrophosphorolysis data. [h] Data from KINSIM fits to k_{cat} and K_M hydrolysis data (Kuchta et al., 1988).

Scheme II

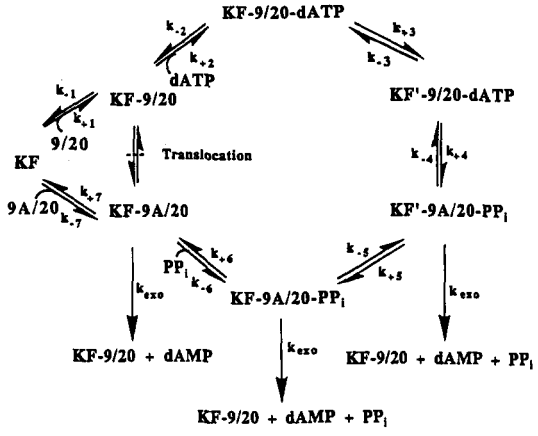

into either HCl or EDTA (Figure 4). Both the burst rate and the burst height are identical when using either the 1.0 N HCl [an acid concentration which has been shown to quench quantitatively the KF(exo+) (Dahlberg & Benkovic, 1991)], or the 45 mM EDTA quench [an EDTA concentration that does not quench the interconversion of the KF′–D_n–dNTP and KF′–D_{n+1}–PP_i complexes when dNTP is the correct nucleotide (Dahlberg & Benkovic, 1991)]. Since KF(exo+) was used, the burst height only reaches a maximum of 60%, consistent with previously published results (Kuchta et al., 1988). From the identical results for both quench solutions we infer that either there is no significant accumulation of KF′–D_n–dNTP or the two central complexes are slow to interconvert on the time scale of the quench procedure.[2] An additional experiment measured the pre-steady-state burst of misincorporation of dCTP into the 9/20-mer with either an HCl or an EDTA quench using excess KF(exo–) to avoid the effect of exonucleolytic editing on the levels of the central species (Figure 5). The burst rates and amplitudes were identical, indicating that there was no large concentration of a ternary species which could partition into products using

[2] We were unable to eliminate the possibility that the mechanism of EDTA quenching for the correct incorporation may be different from the mechanism for the incorrect incorporation.

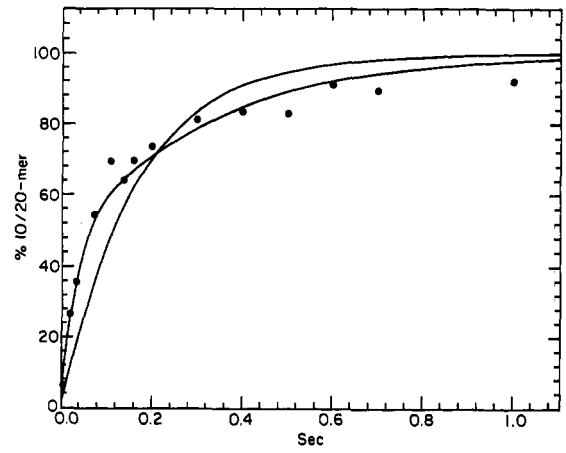

FIGURE 2: Effect of (αS)dATP on the pre-steady-state burst of dTTP incorporation into the 9/20-mer to form the 10/20-mer. Conditions were identical to those in Figure 1 except that the assay contained 125 μM (αS)dATP in place of dATP. The single-exponential fit to the data was generated using sequence 2 of Scheme I and the rate constants in the Figure 1A legend. The double-exponential fit was generated using sequence 3 of Scheme I and the rate constants in the Figure 1B legend.

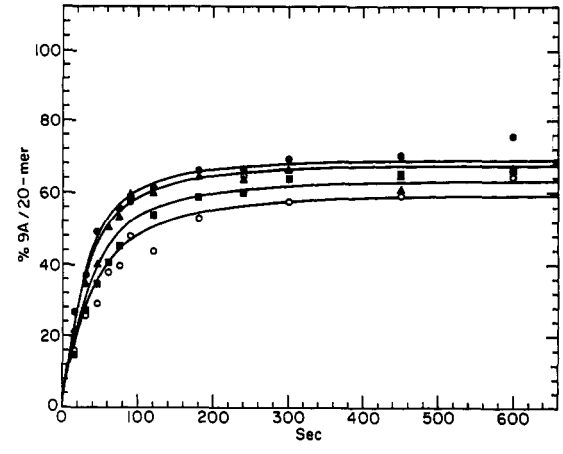

FIGURE 3: Pre-steady-state misincorporation of dATP into the 9/20-mer to form 9A/20-mer. Assays were performed as described under Experimental Procedures with (○) 30, (■) 50, (▲) 125, or (●) 250 μM dATP. The lines were generated by computer simulation using the mechanism in Scheme II and the rate constants in Table I.

the EDTA quench. The burst heights both reached 100%, as found with dATP misincorporation using KF(exo–) (Eger et al., 1991). There was rapid incorporation of two additional dCTPs that form correct base pairs at positions 11 and 12 of the 9/20-mer.

Pyrophosphate Off-Rate from the KF(exo–)–9A/20-PP_i. The rate of pyrophosphate release from the KF(exo–)–9A/20-PP_i complex was measured for a single turnover under polymerizing conditions at outlined in Scheme III. This reaction scheme consists of ordered binding of 9/20-mer and dATP, followed by chemistry and ordered dissociation of pyrophosphate and 9A/20-mer. For the released pyrophosphate concentrations to be measured accurately, the pyrophosphate was hydrolyzed by inorganic pyrophosphatase, generating phosphate. The KF(exo–) mutant was used to limit the amount of pyrophosphate produced from dATP that was initially misincorporated but later removed by the 3′→5′ exonuclease activity.

Several control experiments were performed to ensure that the rate of pyrophosphate release was measured accurately. First, the residual exonuclease activity of the KF(exo–) was measured in a reaction containing 5′-^{32}P-end-labeled 9/20-

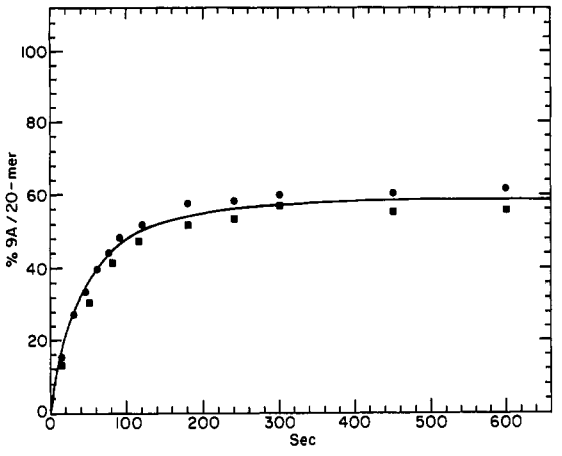

FIGURE 4: Effect of acid or EDTA quench on the pre-steady-state burst of 9A/20-mer formation. Assays were performed with excess KF(exo+) and either an (■) HCl (1.0 N final) or (●) EDTA (45 mM final) quench as described under Experimental Procedures. The line was generated by computer simulation using the mechanism in Scheme II and the rate constants in Table I.

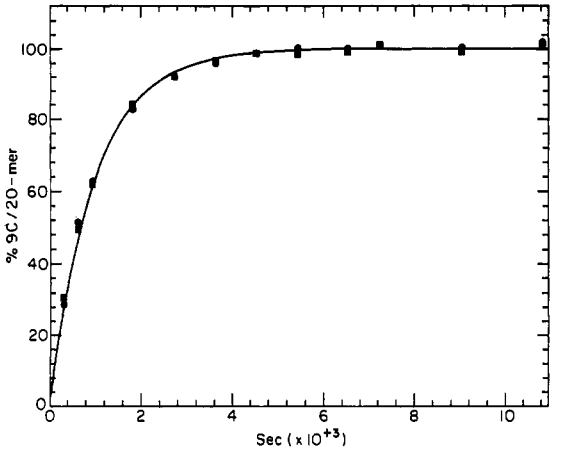

FIGURE 5: Effect of acid or EDTA quench on the pre-steady-state burst of 9C/20-mer formation. Assays were performed with excess KF(exo–) and 30 μM dCTP as described under Experimental Procedures with either an (■) HCl (1.0 N final) or (●) EDTA (45 mM final) quench. Data were fit to sequence 1 of Scheme I with $k_{+1} = 1.2 \times 10^7$ M^{-1} s^{-1}, $k_{-1} = 0.06$ s^{-1}, $k_{+a} = 1 \times 10^8$ M^{-1} s^{-1}, $k_{-a} = 2000$ s^{-1}, and $k_b = 1.7 \times 10^{-3}$ s^{-1}.

Scheme III

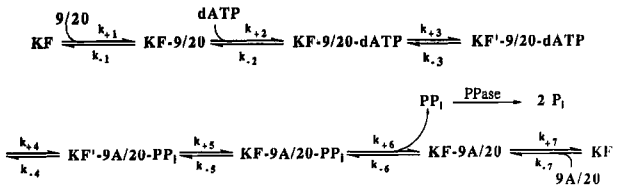

mer, excess KF(exo–), and $MgCl_2$. Second, the steady-state parameters for the pyrophosphatase were determined to ensure that the enzyme would turn over at a high enough rate to couple with the pyrophosphate release. Double-reciprocal analysis of the steady-state rates (data not shown) yielded values of $K_m(PP_i) = 20$ μM and $k_{cat} = 34$ s^{-1}. Computer simulations using these values and the rate constants for misincorporation (Table I) demonstrated that the pyrophosphatase was an adequate coupling enzyme. In addition, the experiments varying the pyrophosphatase concentrations by 3.3-fold showed no change in the measured pyrophosphate release rates. The buildup of free pyrophosphate due to inadequate coupling would be less than the error in the assay points. Third, experiments were performed to assure that

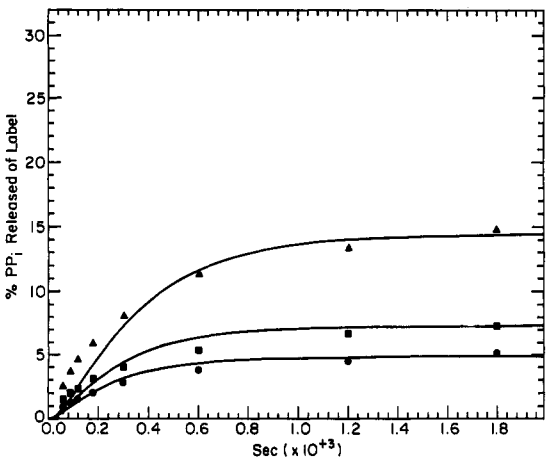

FIGURE 6: Pre-steady-state burst of released pyrophosphate formed as a function of dATP and PP_i concentration. Assays were performed with excess KF(exo–) as described under Experimental Procedures with either (▲) 10, (■) 20, or (●) 30 μM (γ^{32}P)dATP. The data are presented as the percent of PP_i released of the total radiolabel present. The lines were generated by computer simulation using the model in Scheme III and the rate constants in Table I, with the PPase activity modeled by a two-step sequence, where $k_p = 1 \times 10^8$ M^{-1} s^{-1}, $k_{-p} = 2000$ s^{-1}, and $k_{hyd} = 34$ s^{-1}.

$$\text{PPase} + PP_i \underset{k_{-p}}{\overset{k_p}{\rightleftharpoons}} PP_i\text{-PPase} \qquad PP_i\text{-PPase} \xrightarrow{k_{hyd}} 2P_i + \text{PPase}$$

there was adequate quenching of the KF(exo–) and the pyrophosphatase. There is no significant difference, as noted above, in either the burst rate or the burst height of 9A/20-mer formation in pre-steady-state experiments quenched by either HCl (1.0 N) or EDTA (45 mM). In addition, the results of the pyrophosphate off-rate experiment also were independent of the chemical nature of the quench. The destruction of pyrophosphatase activity by acid–chloroform and then neutralization treatments was confirmed by total recovery of radiolabeled pyrophosphate added to the acid quench solution.

Accurate quantitation of the reaction products (P_i vs PP_i and dATP) depends on their stability toward the reaction conditions and complete separation. The three products degraded <0.2% during the time before neutralization of the quench mix or during workup after the addition of chloroform as shown by recovery of added (^{32}P)PP_i and (γ^{32}P)dATP under the TLC conditions used.

The pre-steady-state formation of the released pyrophosphate accompanying the incorporation of dATP into the 9/20-mer to form the 9A/20-mer (measured as P_i) is shown in Figure 6 and occurs at a rate slower than 9A/20-mer formation. Placement of the PP_i release before a slow conformational change step does not predict the slower formation of PP_i relative to formation of 9A/20-mer. Previous data had demonstrated that a slow step, on the order of 5×10^{-3} s^{-1}, was necessary following chemistry (Kuchta et al., 1988). The pyrophosphate release data require a slow step preceding the release of PP_i, i.e., the ordered sequence of steps designated k_5 and k_6 in Scheme II, and provide an evaluation of its magnitude (k_{+5} of Scheme II).

Pyrophosphorolysis on the 9A/20-mer. The KF(exo–) mutant was used to measure the pyrophosphorolysis rate on the 9A/20-mer. The pyrophosphorolysis parameters for KF(exo–) on the 9A/20-mer were $K_m = 800$ μM and $k_{cat} = 7.0 \times 10^{-5}$ s^{-1} (Figure 7). The observed rate of 3′→5′ exonuclease activity was also measured, and each pyrophosphorolysis reaction was corrected for this background rate. Using the previously measured catalytic efficiency for the

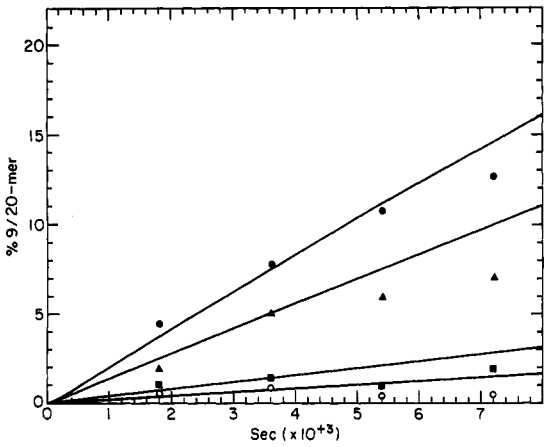

FIGURE 7: Pyrophosphorolysis on the 9A/20-mer to form 9/20-mer. Assays were performed with excess KF(exo–) as described under Experimental Procedures with either (○) 50, (■) 100, (▲) 500, or (●) 1000 μM PP_i. The lines were generated by computer simulation using the model in Scheme II and the rate constants in Table II.

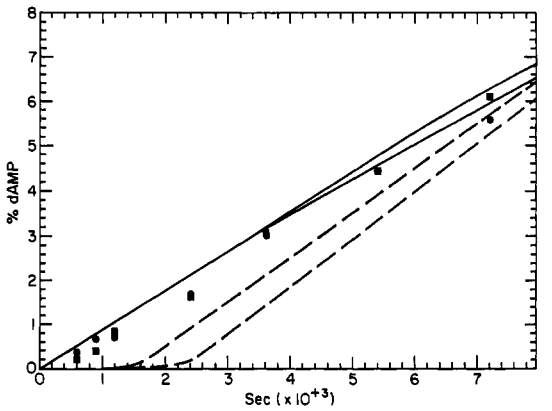

FIGURE 8: Nucleotide turnover with excess DNA over enzymes. Assays were performed as described under Experimental Procedures with either (●) 1.0 or (■) 1.5 μM 9/20-mer. The two dashed lines were generated from Scheme II, which was altered to provide an additional dissociation step of 9A/20-mer directly from the KF'-9A/20-mer-PP_i complex. Given the rate constants used (Table I),

$$\text{KF'-9A/20-mer-PP}_i \underset{k_{-7}}{\overset{k_{+7}}{\rightleftharpoons}} \text{KF'-PP}_i + \text{9A/20-mer}$$

no KF transits the k_{+5} step. The two dashed lines result from initial concentrations of 1.0 (upper) and 1.5 μM (lower) 9/20-mer. The two solid lines were computer simulated using Scheme II and the rate constants in Table I with upper (1.5 μM) and lower (1.0 μM) lines nearly independent of 9/20-mer levels.

misincorporation of dATP into the 9/20-mer (k_{cat}/K_m = 2.5 × 10^2 M^{-1} s^{-1}) (Kuchta et al., 1988), an equilibrium was calculated for the incorporation of dATP into the enzyme-bound 9/20-mer to form enzyme-bound 9A/20-mer plus free pyrophosphate (K_{eq} = 2900 ± 1000).

Nucleotide Turnover. The occurrence of the slow conformation change prior to pyrophosphate release may also be manifest in a slower dissociation of the 9A/20-mer from the KF'–9A/20-mer–PP_i complex that is produced in the chemical step. Previous experiments (Kuchta et al., 1988) suggested that nucleoside monophosphate accumulated at rates exceeding formation of misincorporated DNA product. The rate of dATP turnover to dAMP during 9A/20-mer synthesis at two levels of 9/20-mer is shown in Figure 8. The data are adequately fit by invoking exonucleolytic cleavage of the 9A/20-mer within the KF'–9A/20-mer–PP_i and KF–9A/20-mer species using Scheme II and the rate constants in Table I. Modeling the data using a sequence in which the dissociation rate constant of the 9A/20-mer from the KF'–9A/20-mer–PP_i complex is assumed equal to that for KF–9A/20-mer predicts a variable 9/20-mer concentration-dependent lag in dAMP formation (Figure 8) that was not observed. Given the rapid release rates of the 9A/20-mer (3.25 s^{-1}) as measured previously (Kuchta et al., 1988) and PP_i (8 × 10^4 s^{-1}) as well as the insignificant binding of PP_i at the low experimental PP_i concentrations, the exonucleolytic editing would only occur for this latter sequence at the level of the KF–9A/20-mer complex and would not adequately account for the dAMP produced. Consequently, the rate of escape of 9A/20-mer from the ternary product complex is slowed.

DISCUSSION

The previously determined kinetic mechanism for the misincorporation of a single dATP into a DNA of a defined sequence (9/20-mer) (Kuchta et al., 1988) has been refined to incorporate results from nucleotide discrimination, pyrophosphate release, and pyrophosphorolysis experiments. These measurements have enabled us to detect a conformational change preceding chemistry, to insert a slow conformational change preceding pyrophosphate release, and to calculate the overall equilibrium constant of the reaction. Our expanded kinetic mechanism is presented in Scheme II with the magnitude of the individual steps presented in Table I. The sequence begins with ordered binding of 9/20-mer and dATP followed by a conformational change preceding chemistry. After chemistry, there is a slow conformational change followed by pyrophosphate release before dissociation of 9A/20-mer. The resultant scheme conforms to that independently determined for the correct incorporation of nucleotide in terms of the number and nature of the individual steps.

Nucleotide Binding. In our nucleotide discrimination experiments, we have confirmed the presence of a conformational change preceding chemistry, previously postulated for correct nucleotide incorporation on different experimental grounds (Kuchta et al., 1987; Dahlberg & Benkovic, 1991). Studies on the binding of an incorrect nucleotide (dATP), at levels of 50–250 μM, to the KF(exo+)–9/20-mer complex measured through its effect on the pre-steady-state rate of incorporation of the correct nucleotide (dTTP) provided data that were not adequately fit by sequence 2 of Scheme I, which contains a single dATP binding step.

An alternative model in which dATP binds in two steps preceding the chemical step of dAMP transfer (sequence 3 of Scheme I) describes the present data as well as those determined in the steady state. The initial binding of dATP is weak (k_{-2}/k_2 = 0.17 mM); the second step features a forward rate rapid enough to initially partition the binary KF–9/20-mer species in favor of the ternary KF'–9/20-dATP species. The slower segment in the biphasic kinetics is then governed by the return rate of the ternary species (k_{-3}).

An alternative two-step binding scheme, containing a dead-end species shown as sequence 4 of Scheme I, was eliminated because it will not rationalize both the biphasic discrimination data and the binding constant of dATP (K_m = 8.3 μM) (Kuchta et al., 1988). Moreover, the absence of inhibition at high levels of dATP (Figure 3) also rules against a tight dead-end species.

The contribution of nucleotide discrimination to replication fidelity, as measured by the ratio K_I/K_D, was previously shown to be in the range 0–23-fold, depending on the DNA sequence and the competing nucleotide (Eger et al., 1991). It is likely that this discrimination against an incorrect nucleotide is divided into two steps and these steps parallel the two found

for conversion of the ternary complex containing a correct nucleotide to an active species. The lack of nucleotide selectivity is in sharp contrast to the >100-fold discrimination found for the DNA polymerase from T7 phage (Wong et al., 1991) and T4 phage (Capson and West, unpublished results).

Elemental Effect. Since these nucleotide discrimination experiments examine the binding of the incorrect nucleotide to the enzyme–DNA complex, they are ideally suited to examine the effect of an α-thio substitution on the binding of dATP. Figure 2 demonstrates that (αS)dATP binds to the KF(exo+)–9/20-mer complex with the same biphasic kinetics as the binding of dATP (Figure 1B). Moreover, the rate constants used to model the data for dATP also accurately model (αS)dATP binding.

There are three factors which might have been expected to affect the binding of the (αS)dATP to the KF–9/20-mer complex relative to the dATP. First, from studies on ATP, the α-oxo substrate contains 50–60% tridentate Mg^{2+} coordination in solution (Huang & Tsai, 1982), while the α-thio nucleotide contains only 27% tridentate coordination (Pecoraro et al., 1984). Second, there is also a change in the size of the substituent when oxygen is replaced with sulfur (van der Waals radii of 1.40 vs 1.85 Å). The greater size of the sulfur atom might weaken the binding of the α-thio nucleotide relative to the α-oxo nucleotide through steric interactions (Cohn, 1982). Third, thio substitution lowers the electronegativity of the α-phosphorus atom (Benkovic & Schray, 1971), which might affect important binding interactions in the KF active site. The lack of a change in the binding of the nucleotide when it contains an α-thio substituent suggests that the interactions with the enzyme in this region of the nucleotide are weak within the initial complex.

There is, however, a moderate elemental effect of 20 (measured at a single nucleotide concentration) on the pre-steady-state misincorporation of (αS)dATP when KF(exo–) is used (Eger et al., 1991) and a larger value of 65 for KF(exo+) owing to the complication of accounting for the elemental effect on the latter's exonuclease activity (Gupta et al., 1984). Direct measurement of the pre-steady-state burst of the $9A^s$/20-mer formation at various (αS)dATP levels provided a check on our discrimination experiments and generated a K_M value of 25 ± 4 μM for (αS)dATP (data not shown). This binding constant (since $K_M = K_D$) was within experimental error of the constant (22 μM) modeled from the data in Table I for (αS)dATP and dATP. The measured k_{cat} for (αS)dATP of 0.0020 ± 0.0004 s^{-1} is therefore a direct measure of the influence of sulfur substitution on steps following nucleotide binding and include chemistry or later steps. The elemental effect, calculated from the ratio of the rate of dATP incorporation (0.025 s^{-1}) and the rate of (αS)-dATP incorporation, is 12.5. Recent work on model compounds has focused on the attack at phosphorus of methyl 2,4-dinitrophenyl phosphate and methyl 2,4-dinitrophenyl phosphorothioate by a series of nucleophiles (hydroxide, fluoride, nicotinamide, formate, and pyridine) (Hershlag et al., 1991). The elemental effects measured between 4.1 and 11 were proposed to be a full effect on the chemistry rate. The elemental effect of 12.5 observed here for Klenow fragment misincorporation is consistent with an intrinsic effect on the chemical step, suggesting no additional steps mask the effect and in accord with the variation in the elemental effect for correct incorporation for a series of active site mutants (Polesky et al., 1992).

Pyrophosphate Off-Rate. The rate of release of pyrophosphate from the KF(exo–)–9A/20-PP_i ternary species was measured under polymerizing conditions using a coupled enzyme assay system to measure the concentration of the released pyrophosphate as P_i. To be certain that the pyrophosphate concentration was accurately measured, several control experiments were performed on the coupled enzyme assay system. Since recent work on the pre-steady-state rate for correct nucleotide incorporation into a short DNA showed that >0.8 N HCl but not EDTA traps intermediate species such as E′–DNA–dNTP and E′–DNA–PP_i (EDTA allows their interconversion) along the reaction pathway (Dahlberg & Benkovic, 1991), we conducted a similar examination of the burst of misincorporation of dATP into the 9/20-mer with either an EDTA quench (45 mM) or an HCl quench (1.0 N). There is no significant difference between the two quenches (Figure 4). If we presume the ternary complexes in the present case behave similarly, these results would appear to eliminate two mechanistic possibilities: (i) that there is a KF′–9/20–dATP ternary species at high concentration which will undergo misincorporation following the EDTA quench (this would have been shown by a larger EDTA burst height than that of the acid quench); and (ii) that there is a KF′–9A/20–PP_i ternary species that may undergo pyrophosphorolysis following the EDTA quench (this would have generated a smaller EDTA burst height than that of the acid quench). We conclude that our measurements are not biased by the nature of the quenching medium.

To important features were observed for the formation of released pyrophosphate (Figure 6): (i) the rate of free pyrophosphate formation exhibits only a short lag; and (ii) the rate of free pyrophosphate formation is slower than 9A/20-mer formation (Figures 3 and 6). Given the high K_M for pyrophosphate binding to KF–DNA (K_M = 800 μM), this slower rate of formation of free pyrophosphate relative to 9A/20-mer requires that pyrophosphate release follows a slow conformational change.

Analysis of the Kinetic Mechanism. The complete kinetic scheme for dATP misincorporation is presented in Scheme II, and the rate constants are given in Table I. The binding constant for 9/20-mer (step 1) had been previously measured (Kuchta et al., 1987). The rate constants for steps two and three were determined from nucleotide discrimination experiments. The rate of the k_{+3} step (50^{-1}) was arbitrarily set equal to that measured previously for the interconversion of the initial ternary complex KF–DNA–dNTP to the active ternary complex KF′–DNA–dNTP for correct incorporation (Kuchta et al., 1987), thereby sequestering a significant quantity of the KF–9/20-mer as the KF–9/20-mer–dATP complex and preventing its binding to the dTTP.[3] The slow return rate (k_{-3} = 6.5 s^{-1}) generates the second phase in the pre-steady-state incorporation which is dominated by this return rate. Since the nucleotide binding rate ($k_{+2} = 1 \times 10^8$ M^{-1} s^{-1}) is assumed to be diffusion controlled, the overall binding constant for dATP was used to uniquely determine the nucleotide off-rate from the relationship K_D(dATP) = 22 μM = $k_{-2}k_{-3}/k_{+2}k_{+3}$. Thus, each of the steps in the two-step binding of dATP has been uniquely determined. Because of the slow chemistry rate (k_{+4}) relative to the rates in the two-step dATP binding, the K_M measured in pre-steady-state experiments is equal to the K_D.

[3] The collective data provide a value for the ratio k_{-2}/k_{+3} but not for steps k_{-2} or k_{+3} separately. However, since the relative ground states for KF-D and KF′–D–N are set by the measured K_D (dATP) and k_{-3} is evaluated directly, only the relative level of KF–D–N is not defined (Figure 9). For simplicity and in the absence of data to the contrary, we have assumed the value of k_{+3} is unchanged from its direct measurement in correct nucleotide incorporation.

Table II: Comparison of Experimental and Computer-Modeled Data

constant	exptl data[a]	modeled data[b]
k_{cat}(misincorporation) (s^{-1})	2.1×10^{-3}	3.5×10^{-3}
K_m(misincorporation) (μM)	8.3	10
k_{cat}(hydrolysis) (s^{-1})	5.6×10^{-3}	8.0×10^{-3}
K_m(hydrolysis) (μM)	16	10
K_{eq}	2900 ± 1000[c]	13000[d]

[a] Data from Kuchta et al. (1988). [b] Data were modeled using KINSIM. [c] Calculated from $[k_{cat}(dATP)/K_M(dATP)]/[k_{cat}(PP_i)/K_M(PP_i)]$. [d] Calculated from $(k_{+2}/k_{-2})(k_{+3}/k_{-3})(k_{+4}/k_{-4})(k_{+5}/k_{-5})(k_{+6}/k_{-6})$.

The rate constants for the chemistry step (k_{+4}, k_{-4}) are uniquely determined in the forward direction from data for both the pre-steady-state burst rates of dATP misincorporation (Figure 3) and the pre-steady-state burst of pyrophosphate release (Figure 6). The value of the conformational change (k_{+5}) was determined by the pre-steady-state rate of release of pyrophosphate from the product complex. The reverse of the conformational step (k_{-5}) was determined by the rate of pyrophosphorolysis and is slow relative to the reverse of chemistry (k_{-4}). Pyrophosphate binding (K_6) is also uniquely fit from the pyrophosphorolysis experiments. The binding of pyrophosphate to the KF–9A/20-mer complex was shown to be weak, $K_m(PP_i) = 800$ μM; assuming it to be diffusion controlled ($k_{-6} = 1 \times 10^8$ M^{-1} s^{-1}), the off-rate of pyrophosphate was set at 8.0×10^4 s^{-1}. Finally, the rates for 9A/20-mer dissociation (k_{+7}) and 3′→5′ exonuclease activity on the 9A/20-mer were previously determined from a trapping experiment and by a direct measure of exonuclease activity on the 9A/20-mer, respectively (Kuchta et al., 1988). As a check, the simulation of Scheme II using the rate constants in Table I generated values for the rate of misincorporation, the exonuclease activity, and the internal equilibrium (Table II). These values are within experimental error of the previously published data.

Free Energy Profile and Fidelity. The data which we obtained support and extend our previously published mechansim for misincorporation by the Klenow fragment (Kuchta et al., 1988), which was generalized to longer DNA template-primers (M13 template/30-mer primer) (Eger et al., 1991). We now present a more detailed examination of how the KF polymerase achieves its fidelity by comparing on a step by step basis the addition of correct (Dahlberg & Benkovic, 1991) or incorrect nucleotides (dTTP or dATP) into short template-primer substrates. The two processes are represented by the steps in Scheme II and illustrated in terms of a free energy reaction coordinate diagram (Figure 9); the minimal kinetic sequences for either correct or incorrect incorporation use the same ordering and number of kinetic steps.

The nucleotide (correct or incorrect) binds to the KF–D complex in a two-step process leading to the active ternary complex, KF′–D–N. The contribution of nucleotide binding to fidelity is in general small (1–23-fold for various sequences), with the difference between the KF′–D–N complexes in this case being ca. 2 kcal/mol. We have presumed that the magnitude of the conformational change that interconverts inactive KF–D–N and active KF′–D–N is identical for correct incorporation and misincorporation; this presumption provides an adequate fit to our data. It is clear that the major contribution to replication fidelity in the first step still resides in the chemical step, which provides an increased free energy barrier of minimally 6 kcal/mol for the addition of dATP vs dTTP. The value of the rate constants (k_{+4} and k_{-4}) for the chemical step for dTTP incorporation has not been determined; however, this step is at equilibrium so that k_{+4} and k_{-4} must

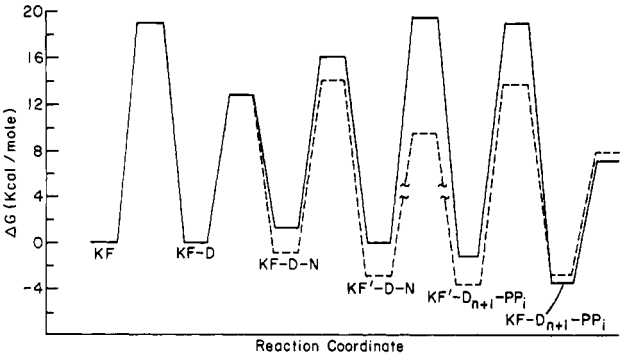

FIGURE 9: Free energy profile for correct and incorrect nucleotide incorporation by the Klenow fragment. The free energy for each reaction step (Table I) was calculated from $\Delta G = RT[\ln(kT/h) - \ln(k_{obs})]$, where R is 1.99 cal K^{-1} mol^{-1} (gas constant), T is 295 K, k is 3.30×10^{-24} cal K^{-1} (Boltzmann's constant), h is 1.58×10^{-34} cal s (Planck's constant), and k_{obs} is the first-order rate constant given in Table I. The concentrations used were 5 nM 9/20-mer and 22 μM dATP. Solid lines are the free energies presented in Table I for misincorporation of dATP into the 9/20-mer to form 9A/20-mer. The dashed lines are the free energies for correct nucleotide incorporation into the 13/20-mer to form 14/20-mer calculated for 5 nM 13/20-mer and 22 μM dATP (Dahlberg & Benkovic, 1991). Inclusion of the binding of the incorrect nucleotide into the computer simulations gave revised values of $K_D^{PP_i} = 800$ μM, $k_{+5} = 1.0$ s^{-1}, and $k_{-5} = 4$ s^{-1} (Dahlberg, 1992). The scheme represents steps in the misincorporation reaction presented in Scheme II, which are also analogous to the steps for correct incorporation (Dahlberg & Benkovic, 1991).

exceed 200 s^{-1} (Dahlberg & Benkovic, 1991). Overall, the contribution to fidelity imposed by the free energy barrier in the chemical step provides discrimination factors of 10^4–10^6 for various sequences (Kuchta et al., 1988).

The second stage of discrimination is imposed by the barrier to pyrophosphate loss from the KF′–D_{n+1}-PP_i complex that proceeds in two steps. The rate ($k_5 = 6 \times 10^{-3}$ s^{-1}) of conversion of the immediate product ternary complex to one that releases pyrophosphate predominantly sets the steady-state rate for misincorporation, since the $\Delta\Delta G^{\ddagger}$ for this step relative to that for correct incorporation is ca. 6.5 kcal/mol more unfavorable. The consequences of this increased barrier are twofold: (i) editing of the mismatch by interal pyrophosphorolysis ($k_{-4} = 3.0 \times 10^{-3}$ s^{-1}) can compete with the rate of ternary product conversion ($k_5 = 6.0 \times 10^{-3}$ s^{-1}); and (ii) exonucleolytic editing now can occur at the level of the KF′–D_{n+1}-PP_i complex, since the rate (1.1×10^{-2} s^{-1}) of nucleoside formation (dAMP) via exonucleolytic cleavage[4] is also comparable. For either to occur, however, the D_{n+1} cannot readily dissociate from the central ternary complex prior to processing. Simulation of the measurements of nucleotide turnover indeed indicate that the loss of D_{n+1} from KF′–D_{n+1}-PP_i must be less than 1.1×10^{-2} s^{-1}, a dramatic decrease from that observed for KF–9A/20-mer (3.25 s^{-1}). We deduce that the two steps involving conformational changes serve to lock the DNA to the central ternary complexes, allowing for efficient exonucleolytic editing by hydrolysis and, to a lesser extent, for internal pyrophosphorolysis. One might further speculate that the importance of the k_5 step may be inversely proportional to the magnitude of the exonuclease activity to provide an adequate residence

[4] The rate for exonucleolytic editing of the KF–D_{n+1} complex has been directly measured by monitoring the hydrolysis of the primer terminus of the 9A/20-mer and of the KF′–D_{n+1}–PP_i species by a comparison of dATP incorporation using the KF(exo–) and KF(exo+) enzymes (Kuchta et al., 1988; Eger et al., 1991). The values of k_{exo} range from 8×10^{-3} to 12×10^{-3} s^{-1} and appear not to reflect the increased interaction between the enzyme and D_{n+1} in the central complex.

time for hydrolytic editing to occur on the initial misincorporated product complex. In other polymerases with much greater exonuclease activity but lower DNA affinity, such as T4 and T7, this locking step may be achieved by the accessory proteins. The contribution of this second stage to overall replication fidelity for this case is ca. 4-fold.

It is of interest to speculate on the nature of the second conformational change step. Template-primer melting associated with transfer between the polymerase and exonuclease sites would occur in the k_{exo} step and not be seen. However, steric hindrance derived from the A–A mismatch relative to the correct A–T base pair might be reflected in an increased reaction barrier associated with repositioning of the DNA for the next nucleotide incorporation. Thus, after a nucleotide has been misincorporated at the polymerase site, the pyrophosphate is not released until either the base is hydrolyzed (in the first exonuclease step) or the primer has moved into position for the next nucleotide incorporation. Since the binding of pyrophosphate is weak, the contribution of the second exonuclease step to the 9A/20-mer is negligible.

The third stage of replication fidelity, which is not addressed in this paper, involves the slow addition of the next correct nucleotide onto a mismatch which allows the 3′→5′ exonuclease to remove the mismatch. This stage has been shown to contribute a factor of between 6 and 340 to overall replication fidelity (Kuchta et al., 1988). The generality of this stage was demonstrated recently through trapping experiments on several misincorporated DNA products (Joyce, 1989). It is noteworthy that the overall equilibrium (KF–D + N $\rightleftharpoons$ KF–D_{n+1} + PP_i) and the internal equilibrium (KF′–D–N $\rightleftharpoons$ KF′-D_{n+1} + PP_i) are the same for both correct and incorrect nucleotides (Dahlberg & Benkovic, 1991) within the limits of our experimental uncertainty.

Conclusion. The presence of conformational change steps preceding and following the chemistry step has now been established for misincorporation by the Klenow fragment. Nucleotide discrimination experiments have demonstrated the rapid two-step binding of the nucleotide. The release of pyrophosphate as well as the steady-state nucleotide turnover has confirmed the existence of a second conformational change which allows the enzyme additional time for the tightly bound product to be either hydrolytically excised or returned to substrates (internal proofreading). Examination of the elemental effect through nucleotide discrimination experiments has eliminated nucleotide binding as the source of the pre- and steady-state elemental effect. Finally, the measurement of pyrophosphorolysis allowed the refinement of the final rates in the mechanism so that a single unique kinetic mechanism for misincorporation by the Klenow fragment was established.

ACKNOWLEDGMENT

We thank Dr. Catherine Joyce (Yale University) for supplying the KF(exo+) and KF(exo–) clones, Dr. Richard Gibbs for running the ^{31}P NMR, Dr. Jin-Tann Chen for synthesizing the (αS)dATP, and Patricia Benkovic for reading and editing the manuscript.

REFERENCES

Anderson, K. S., Sikorski, J. A., & Johnson, K. A. (1988) *Biochemistry 27*, 7395.

Bambara, R. A., Uyemura, D., & Lehman, I. R. (1976) *J. Biol. Chem. 251*, 4090.

Barshop, B. A., Wrenn, R. F., & Frieden, C. (1983) *Anal. Biochem. 130*, 134.

Benkovic, S. J., & Schray, K. J. (1971) in *The Enzymes* (Boyer, P. D., Ed.) 3rd ed., p 201, Academic Press, New York.

Brody, R. S., & Frey, P. A. (1981) *Biochemistry 20*, 1245.

Brutlag, D., Atkinson, M. R., Setlow, P., & Kornberg, A. (1969) *Biochem. Biophys. Res. Commun. 37*, 982.

Bryant, F. R., Johnson, K. A., & Benkovic, S. J. (1983) *Biochemistry 22*, 3537.

Burgers, P. M. J., & Eckstein, F. (1979) *J. Biol. Chem. 254*, 6889.

Carroll, S. S., & Benkovic, S. J. (1990) *Chem. Rev. 90*, 1291.

Catalano, C. E., & Benkovic, S. J. (1989) *Biochemistry 28*, 4374.

Chen, J.-T., & Benkovic, S. J. (1983) *Nucleic Acids Res. 11*, 3737.

Cohn, M. (1982) *Acc. Chem. Res. 15*, 326.

Cowart, M., Gibson, K. J., Allen, D. J., & Benkovic, S. J. (1989) *Biochemistry 28*, 1975.

Dahlberg, M. E. (1992) Thesis, The Pennsylvania State University.

Dahlberg, M. E., & Benkovic, S. J. (1991) *Biochemistry 30*, 4835.

Derbyshire, V., Freemont, P. S., Sanderson, M. R., Beese, L., Friedman, J. M., Joyce, C., & Steitz, T. (1988) *Science 240*, 199.

Eger, B. T., Kuchta, R. D., Carroll, S. S., Johnson, K. A., Benkovic, P. A., Dahlberg, M. E., & Benkovic, S. J. (1991) *Biochemistry 30*, 1441.

Englisch, U., Gauss, D., Freist, W., Englisch, S., Sternbach, H. S., & von der Haal, F. (1985) *Angew. Chem., Int. Ed. Engl. 24*, 1015.

Freemont, P. S., Friedman, J. M., Beese, L. S., Sanderson, M. R., & Steitz, T. A. (1988) *Proc. Natl. Acad. Sci. U.S.A. 85*, 8924.

Gupta, A. P., & Benkovic, S. J. (1984) *Biochemistry 23*, 5874.

Gupta, A. P., Benkovic, P. A., & Benkovic, S. J. (1984) *Nucleic Acids Res. 12*, 5897.

Hershlag, D., Piccirilli, J. A., & Cech, T. A. (1991) *Biochemistry 30*, 4844.

Huang, S. L., & Tsai, M.-D. (1982) *Biochemistry 21*, 951.

Johnson, K. A. (1986) *Methods Enzymol. 134*, 677.

Joyce, C. M. (1989) *J. Biol. Chem. 264*, 10858.

Joyce, C. M., & Grindley, N. D. F. (1983) *Proc. Natl. Acad. Sci. U.S.A. 80*, 1830.

Joyce, C. M., & Steitz, T. A. (1987) *Trends Biochem. Sci. 12*, 288.

Klenow, H., & Henningsen, I. (1970) *Proc. Natl. Acad. Sci. U.S.A. 65*, 168.

Kornberg, A., & Baker, T. A. (1992) in *DNA Replication*, Freeman, New York.

Kuchta, R. D., Mizrahi, V., Benkovic, P. A., Johnson, K. A., & Benkovic, S. J. (1987) *Biochemistry 26*, 8410.

Kuchta, R. D., Benkovic, P. A., & Benkovic, S. J. (1988) *Biochemistry 27*, 6716.

McClure, W. R., & Jovin, T. M. (1975) *J. Biol. Chem. 250*, 4073.

Mizrahi, V., Henrie, R. N., Marlier, J. F., Johnson, K. A., & Benkovic, S. J. (1985) *Biochemistry 24*, 4010.

Mizrahi, V., Benkovic, P. A., & Benkovic, S. J. (1986a) *Proc. Natl. Acad. Sci. U.S.A. 83*, 231.

Mizrahi, V., Benkovic, P. A., & Benkovic, S. J. (1986b) *Proc. Natl. Acad. Sci. U.S.A. 83*, 5769.

Ollis, D. L., Brick, P., Hamlin, R., Xuong, N. G., & Steitz, T. A. (1985) *Nature (London) 313*, 762.

Pecoraro, V. L., Hermes, J. D., & Cleland, W. W. (1984) *Biochemistry 23*, 5262.

Polesky, A. H., Dahlberg, M. E., Benkovic, S. J., Grindley, N. D. F., & Joyce, C. M. (1992) *J. Biol. Chem. 267*, 8417.

Setlow, P., Brutlag, P., & Kornberg, A. (1972) *J. Biol. Chem. 247*, 224.

Wong, I., Patel, S. S., & Johnson, K. A. (1991) *Biochemistry 30*, 526.